Pressure based active load control of a blade in dynamic stall conditions

Barrio, J. Fernández; Mertens, C.; Ragni, D.; Sciacchitano, A.; Van Oudheusden, B.

DOI
10.1088/1742-6596/1618/2/022003

Publication date
2020

Document Version
Final published version

Published in
Journal of Physics: Conference Series

Pressure based active load control of a blade in dynamic stall conditions

Pressure based active load control of a blade in dynamic stall conditions

J. Fernández Barrio, C. Mertens, D. Ragni, A. Schiacchitano and B. van Oudheusden

Faculty of Aerospace Engineering, Delft University of Technology, 2629HS Delft, The Netherlands

E-mail: jorgefeb94@gmail.com

Abstract. A proportionate controller is investigated experimentally for unsteady load alleviation purposes on a 2D wing model with a trailing-edge flap. The controller acts on the velocity of the flaps, and pressure sensors are used to detect the unsteady loads, which are generated by actuating the wing model in a sinusoidal motion. Two different regimes are considered: attached flow and dynamic stall. The influence of actuation frequency and controller time lag is also studied. A reduction of 87.5% in the standard deviation of the lift is obtained for a frequency of 0.2Hz and time lag in the control system of 12ms for attached flow conditions. The reduction of the standard deviation of the lift deteriorates for increased frequency and time lag. The proposed controller is also able to reduce the loads during dynamic stall, although the reduction is smaller, close to 40%, and can negatively affect the aerodynamic damping of the model. The flap actuation is also shown to delay the onset of dynamic stall, by increasing the static stall angle with respect to the case without flap deflection.

1. Introduction

The increasing demand on wind energy production has resulted in an increase on wind turbine size, as the power extracted scales quadratically with wind turbine size. This upscaling is limited, as the weight scales volumetrically with size [1]. Emphasis should thus be placed in reducing the weight of the different components of the turbine, as this would reduce the gravitational loads on larger wind turbines. However, this could result in susceptibility to fatigue damage [2], due to insteady inflow conditions such as wind shear, turbulence or tower shadow wake. Reducing these unsteady loads is thus necessary if turbines are to become lighter and larger.

The Smart Rotor concept for wind turbines is an existing approach for the reduction of unsteady loads on wind turbine blades [3]. The concept is based on the active control of dynamic loads by actuation of aerodynamic control devices on the rotor blades. While a consensus has been reached in using trailing edge flaps as the actuation device, several control and sensing systems have seen successful implementation, with no specific sensor or control architecture proving to be superior for implementation in a Smart Rotor concept [3].

Unsteady inflow conditions can promote the occurrence of dynamic stall on a Horizontal Axis Wind Turbine (HAWT) [4]. Dynamic stall is an unsteady flow phenomenon, originated by rapid changes in the angle of attack. This promotes the formation of a Leading Edge Vortex (LEV), which keeps the flow attached past the static stall angle, increasing the lift acting on the blade. The LEV eventually detaches, generating a sudden drop in lift followed by a drop in moment.

Large unsteadiness is associated with this phenomenon, as well as susceptibility to aero-elastic instabilities such as flutter [5].

Dynamic stall has not been studied yet in a Smart Rotor concept, even though it generates highly unsteady loads. Most of the research in this area has been focused on the optimal form of control, either with aero-servo-elastic codes [13, 21, 14, 15, 16] or experimental studies, both on wind tunnels [18, 19, 20] and even in full-scaled wind turbines [17]. The load reduction capabilities of a Smart Rotor under dynamic stall have not been tested.

This paper attempts to bridge this gap, by studying the suitability of a simple controller to reduce fatigue loads under dynamic stall conditions on a 2D wing equipped with a trailing edge flap, based on loads integrated from pressure transducers. In order to do this, the proposed controller will be subjected to two different oscillating motions, representative of both attached flow and dynamic stall conditions. Firstly, the experimental setup will be described, followed by the data analysis methodology. After that, the results will be shown, both for attached flow and dynamic stall conditions, followed by a discussion regarding the influence of the time lag, controller gain and actuation frequency.

2. Experimental Setup

The experimental study is carried out in the Open Jet Facility at Delft University of Technology. The 2D wing model is obtained by extrusion of a NACA 0018 profile with chord 0.4 m and span 1.45 m [6], and actuated in a sinusoidal motion in order to generate an unsteady loading, at a constant free-stream velocity of 5m/s ($\mathrm{Re} = 1.3 \times 10^5$). Due to the low Reynolds number, a zig-zag strip is added at $0.1c$, with a thickness of 2 mm, a width of 12 mm and an angle of 60°, to force transition to turbulent flow. Circular side plates with a diameter of 0.8 m are placed at each side of the wing to avoid 3D effects. The experimental setup is shown in figure 1.

The model employs a moveable rigid trailing edge flap, which extends over the entire span with a length of $0.25c$, serving as the Smart Rotor actuator. 24 differential pressure transducers are installed inside the model, for measuring the loads acting on the model, thus comprising

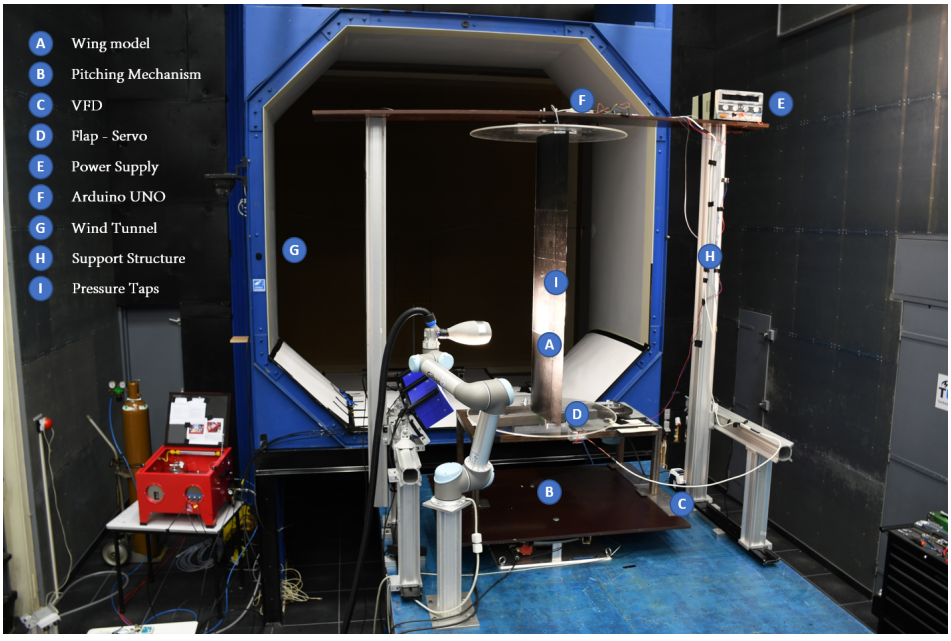

Figure 1. General Setup employed during the experiments

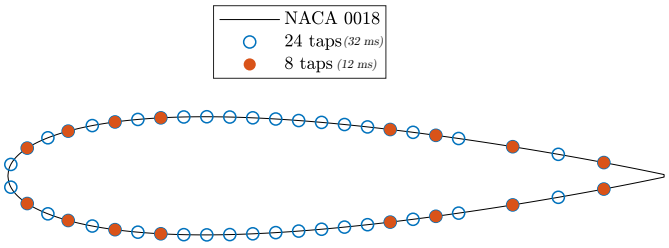

Figure 2. Position of the pressure taps for the 24 pressure tap integration scheme and the 8 pressure tap integration scheme

the sensing system. The pressure sensor signals are transmitted serially to an Arduino UNO board, and sent forward to a LabView project in order to integrate the lift and moment acting on the model. In view of the serial communication, two different integration schemes are used, employing either all 24 or only 8 pressure taps, which result in a time lag in the control system of 32 and 12 ms respectively. The taps employed for the different control schemes are indicated in figure 2. The integrated C_l is fed into a proportionate controller, which generates a signal for the velocity of the flap ($\dot{\beta}$) based on the deviation of this C_l with respect to the Set Point (SP), and the value of the proportional gain K_p, as seen in equation 1. The controller acts on the C_l since the focus of the Smart Rotor research area is to reduce the bending moment acting on the blade, although this is expected to deteriorate the torsional fatigue due to the increased moment oscillations.

$$\dot{\beta} = K_p(C_l - SP) \tag{1}$$

The unsteady inflow conditions are generated by a pitching mechanism, that rotates the wing around its pitching axis at 0.3125c. The mechanism transforms the angular motion of a rotating shaft driven by an AC motor into a sinusoidal motion by means of a linkage mechanism. A flywheel is installed on the rotating shaft, where one end of a linkage bar is fixed at a certain distance from the rotation axis. The other end of the linkage bar is attached to the lower side plate of the wing model. With this linkage mechanism, the rotation of a shaft is converted into a motion that resembles a purely sinusoidal motion. The maximum difference of the motion generated by the piching mechanism and a purely sinusoidal motion is 0.07° for an amplitude of oscillations of 4°.

The mechanism was operated at different reduced frequencies ($k = \pi f V_{inf}/c = 0.05, 0.1, 0.2$) with an amplitude of 4°. The frequency of oscillations was controlled with a Variable Frequency Drive (VFD). Two different mean angles of the oscillations were considered: 0.25°, where no large separation is expected, referred as attached flow from now on; and 15.75°, where dynamic stall occurs. A total of 12 runs were performed, for each combination of regime, frequency and time lag. For each run several values of the controller gain K_p were tested, each one for 120 seconds, and the data from the pressure transducers was stored for further analysis.

Table 1. Parameters of the Experiment

Parameter	Symbol	Value
Velocity	V_∞	5 m/s
Chord	c	0.4 m
Span	s	1.45 m
Reynolds number	Re	1.3×10^5
Mean angle of oscillations	α_0	0.25° 15.75°
Amplitude of oscillations	α_{amp}	4°
Oscillations frequency	f	0.2Hz 0.4Hz 0.8Hz
Reduced frequency of oscillations	k	0.05 0.1 0.2
Time lag	τ	32 ms 12ms

3. Methodology

The pressure data stored during the experiments is phase-averaged, and the uncertainty of the phase-averaged results with 95% confidence interval calculated following the procedure described by Moffat [7]. For the dynamic stall case, the small amplitude of oscillations and the stochastic nature of flow reattachment resulted in some of the cycles not recovering from stall. These cycles are filtered out,as they are not representative of dynamic stall conditions. The reduction in number of cycles increases the uncertainty in the phase-averaged results during this regime.

The effectiveness of the controller to reduce the unsteady loads acting on the wing model is assessed by comparing the standard deviation of the C_l in the controlled cases ($K_p \neq 0$) with the baseline case ($K_p = 0$). Instabilities are found at large values of K_p, so a spectral analysis is carried out, performing the Fourier transform of the C_l signal, to identify the effect the active control has on the frequency spectrum, and the origin of the instabilities.

Besides the large load oscillations found during dynamic stall, the non-linear aerodynamics may cause the wing to extract energy from the flow [12]. This can be quantified by means of the cycle aerodynamic damping (Ξ_{cycle}), which is derived for a pitching airfoil [5]. Negative values indicate that energy is being extracted from the flow, and therefore the wing may experience aero-elastic instabilities such as flutter. The effect that the control has on the aerodynamic damping is a significant parameter to study, both in attached flow and dynamic stall conditions. This is done by looking at the extra contribution to the aerodynamic damping (Ξ_{cycle_f}) due to the flap actuation, by dividing the C_m into the contribution of the baseline case $C_{m,0}$ and the contribution due to the flap actuation $C_{m,f}$, as is shown in equation 2.

$$\Xi_{cycle} = -\frac{1}{\pi \alpha_{amp}} \oint (C_{m,0} + C_{m,f})\, d\alpha = \Xi_{cycle_0} + \Xi_{cycle_f} \tag{2}$$

Since dynamic stall is a leading-edge phenomenon, the trailing edge flap actuation is expected to have minimal effect in the cycle development [9]. This will be quantified by looking at the Dynamic Stall onset, which is the point at which the LEV detaches from the surface of the wing model. Surface pressure data can be used to estimate the dynamic stall onset, following the procedure of Sheng et al [10].

4. Results

A static characterization of the wing model is carried out as a preliminary part of the experiment. Wind tunnel corrections have been applied to the results, due to the lift interference of the model in the open wind tunnel, that reduces the effective angle of attack. The corrections applied are used following the procedure described by Brooks et al [11]. It can be seen in figure 3 how the

lift slope of the experimental results agrees with the one obtained by a viscous XFOIL analysis performed on the same airfoil at the same Reynolds number, and its smaller than 2D potential theory due to viscous effects. The static stall angle is $\alpha_{ss} \approx 17.5$. The mean angle of oscillations during the dynamic stall regime was chose based on this angle. Lastly, the C_m is higher in the experimental results than in XFOIL, see figure 4, which is ascribed to the zig-zag strip, that increases the effective thickness of the airfoil.

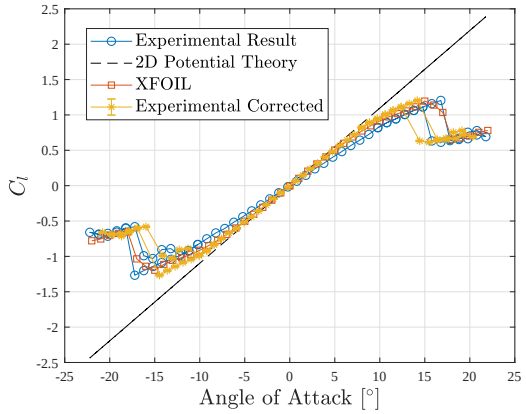

Figure 3. Static lift polar for the Wing model, compared to potential theory and a viscous XFOIL analysis

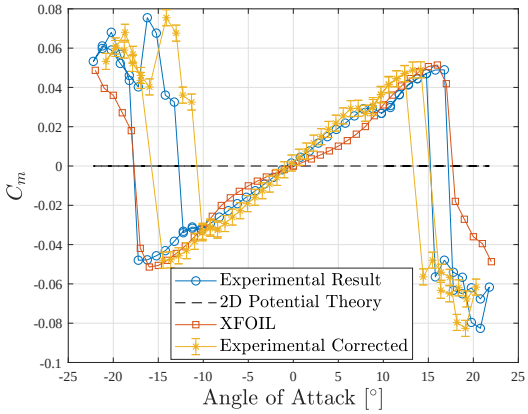

Figure 4. Static moment polar for the Wing model, compared to potential theory and a viscous XFOIL analysis

4.1. Attached flow

After the static characterization of the wing model, the controller performance under unsteady attached flow conditions was tested for different oscillation frequencies and controller time lags. Several values of the controller gain K_p were tested. The SP of the controller is set to 0, i.e. the controller tries to mantain the lift at zero. The phase-averaged results for the frequency of 0.4Hz are shown next. In figure 5 the C_l during the oscillation cycle is presented for the controller based on the integration scheme using 24 pressure sensors, which corresponds to a time lag of 32 ms. In figure 6, the results for the 8 pressure integration scheme with time lag of 12 ms are shown.

The performance of the controller is much better across the range of values of K_p tested for the reduced time lag integration scheme. In any case, the controller is able to reduce the loads, and for each integration scheme there is an optimal value of K_p which corresponds to the largest load variation reduction. Lower values of K_p result in a slower response of the flap, with less compensation of the load variation, while higher values of K_p generate responses that are too fast and lead to excitation of higher frequencies. This can be seen in figure 7, where the Fourier transform of the C_l signal is depicted for the baseline case, as well as for a value of $K_p = -500$ for both integration schemes.

It can be seen that the 1P frequency, in this case 0.4Hz, is largely reduced by both integration schemes. However, the 24 pressure tap integration scheme excites large values of the 4P frequency (1.6Hz), while the 8 pressure tap integration scheme excites frequencies close to the 6P frequency (2.4Hz), but the magnitude is much lower. This behaviour is seen for every frequency, with the 24 pressure tap integration scheme exciting always the 1.6Hz frequency and the 8 pressure tap integration scheme the 2.4Hz frequency. Reducing the time lag in the system makes instabilities less likely, and at higher frequencies.

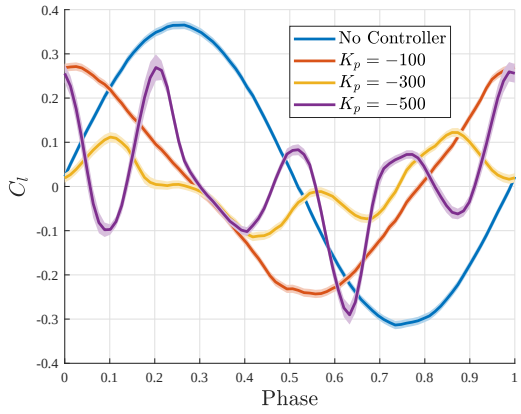

Figure 5. Phase-averaged C_l during the oscillation cycle, for the baseline case and different values of the controller gain K_p. Attached flow with $f = 0.4Hz$ and 24 pressure tap integration scheme. Uncertainty shown by means of the shaded region

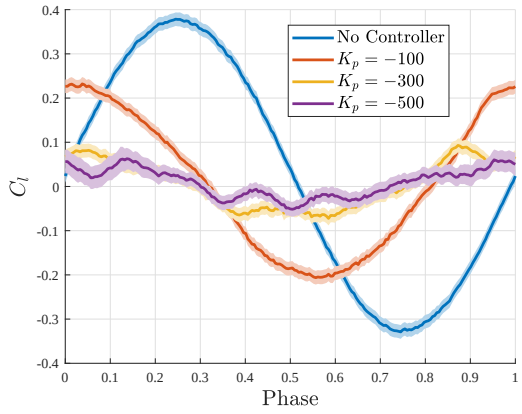

Figure 6. Phase-averaged C_l during the oscillation cycle, for the baseline case and different values of the controller gain K_p. Attached flow with $f = 0.4Hz$ and 8 pressure tap integration scheme. Uncertainty shown by means of the shaded region.

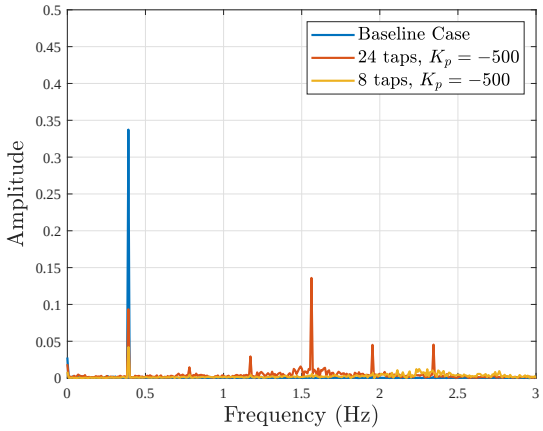

Figure 7. Comparison of the Fourier transform of the C_l signal for the baseline case and the $K_p = -500$ cases for both integration schemes. Attached flow conditions with $f = 0.4Hz$

A summary of the achieved load alleviation, in terms of the reduction of the standard deviation of the C_l, under attached flow conditions is shown in figure 8. It can be seen that reducing the time lag is crucial in the load reduction capabilities of the controller. For the 8 pressure tap integration scheme, a reduction of 87.5% is achieved for the frequency of 0.2Hz, 80% for the frequency of 0.4Hz and 67.5% for 0.8Hz. It can also be seen that the time scale of the excitation, i.e. the oscillation frequency, is important, as higher frequencies require faster actuation responses. Since the frequency of unsteadiness is an imposed condition in the case of a Smart Rotor operation in reality, this indicates that the higher effort should be placed in reducing the time lag present in the system as much as possible.

The results for the aerodynamic damping are shown in figure 9. The damping is positive for the baseline case ($K_p = 0$), while for low values of K_p, which correspond to slow actuations of

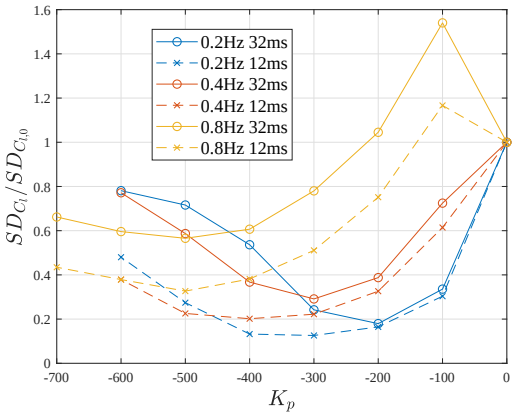

Figure 8. Comparison of the normalized standard deviation of the C_l with respect to the Baseline case, for different frequencies and integration schemes, during Attached Flow

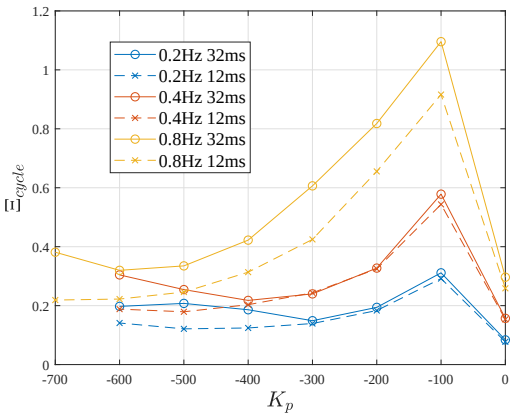

Figure 9. Comparison of the aerodynamic damping, for different frequencies and integration schemes, during Attached Flow

the trailing edge flap, the value of the aerodynamic damping is increased, since the flap motion is lagging behind the pitching motion and this generates an extra positive contribution to it. As K_p increases, the motion of the flap comes closer to the ideal motion, which is expected to be in-phase with the pitching motion. This type of motion has almost no contribution to the aerodynamic damping.

4.2. Dynamic stall

For the dynamic stall conditions, a SP of 1.1 is chosen, since this is the mean value of the C_l observed during the baseline case. It should be noted that the case of 0.8Hz is not shown here, since the LEV detaches mid-downstroke, generating load variations that are not representative of a typical dynamic stall cycle. It will be used however when assessing the onset of dynamic stall. The optimal reduction of the standard deviation of the C_l is around 40% for both integration schemes at the frequencies of 0.2Hz and 0.4Hz. This is ascribed to the higher range of loads appearing, with a difference between $C_{l,max}$ and $C_{l,min}$ of more than 1. The flap cannot compensate for this, and saturates at $\pm 10^{\circ}$ before and after the detachment of the LEV. This also explains the similar values of load reduction for different time lags.

The benefits of the reduced time lag can be seen however in figures 10 and 11, and quantified in table 2, for the dynamic stall configuration at 0.4Hz. Although the values of standard deviation of C_l are similar, the 8 pressure tap integration scheme reduces the peak-to-peak loads experienced during the detachment of the LEV. This occurs because the drop in lift is detected earlier with the reduced time lag, and the flap reacts accordingly. It should also be noted that values of K_p larger than -200 saturate the velocity of the flap. The flap moves at its maximum actuation velocity, and not at the motion prescribed by the controller. In order to maximise the effectiveness of the Smart Rotor in dynamic stall conditions, the time lag should be reduced, and the actuation system should be as fast as possible. However, it is proven that this controller architecture is able to reduce the loads acting on a blade on a highly non-linear phenomenon such as dynamic stall.

The non-linear characteristics of dynamic stall generate a negative cycle aerodynamic damping for the baseline case (Ξ_{cycle_0}), with a value of -0.97 for 0.2Hz and -1.16 for 0.4Hz. This means that the wing is extracting energy from the flow. This can be thought of as a clockwise loop in the moment coefficient with respect to the angle of attack. The values of

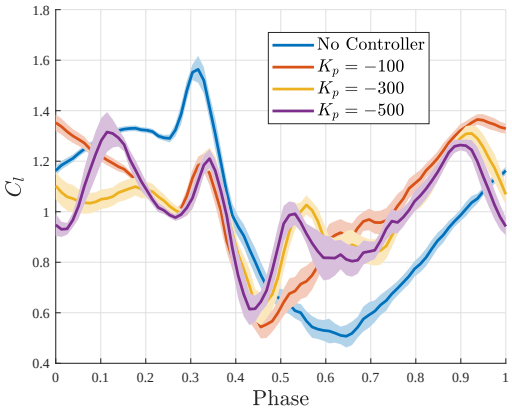

Figure 10. Phase-averaged C_l during the oscillation cycle, for the baseline case and different values of the controller gain K_p. Dynamic stall with $f = 0.4Hz$ and 24 pressure tap integration scheme. Uncertainty shown by means of the shaded region

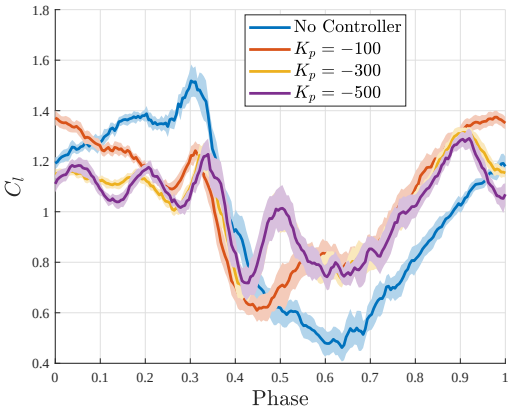

Figure 11. Phase-averaged C_l during the oscillation cycle, for the baseline case and different values of the controller gain K_p. Dynamic stall with $f = 0.4Hz$ and 8 pressure tap integration scheme. Uncertainty shown by means of the shaded region

Table 2. Load reduction parameters for the Dynamic Stall run at 0.4Hz

	Value of K_p for 24 taps				Value of K_p for 8 taps			
	0	-100	-300	-500	0	-100	-300	-500
SD_{C_l}	0.31	0.25	0.19	0.22	0.31	0.26	0.20	0.20
SD_{C_m}	0.06	0.08	0.09	0.09	0.06	0.08	0.09	0.09
$C_{l,max}$	1.56	1.20	1.21	1.21	1.52	1.24	1.22	1.23
$C_{l,min}$	0.51	0.54	0.61	0.61	0.46	0.61	0.70	0.72
C_l *Range*	1.05	0.66	0.60	0.60	1.04	0.63	0.48	0.49

aerodynamic damping are extremely dependent on parameters such as the reduced frequency k, α_0, α_{amp} and even the airfoil geometry [12]. In this case the negative values of the baseline case are thought to appear due to the small amplitude of oscillations. The effect of the controller on this aerodynamic damping can be quantified with equation 2, by evaluating Ξ_{cycle_f}. The $C_{m,f}$ with respect to α is plotted in figures 12 and 13. A clockwise loop equates a negative contribution of the flap to the aerodynamic damping, while a counter-clockwise has a positive effect.

For the frequency of 0.2Hz the flap actuation considerably worsens the aerodynamic damping of the wing, while for 0.4Hz the net contribution is still negative but positive contributions are found during part of the cycle. This effect is strongly dependent on the onset of dynamic stall. For 0.2Hz, this occurs before the start of the downstroke, while for 0.4Hz it happens after. This generates that the drop in lift occurs at different instances during the cycle. Since the controller reaction to the drop in lift is to deflect the flap downwards, which reduces the pitching moment, if this occurs before the downstroke it generates a negative contribution to the aerodynamic damping, as it does with 0.2Hz. This is unfortunately thought to be the most representative case of dynamic stall, with the LEV detaching from the surface during the upstroke [12]. Therefore, even though the Smart Rotor is able to reduce the loads acting on the airfoil, it may be at the

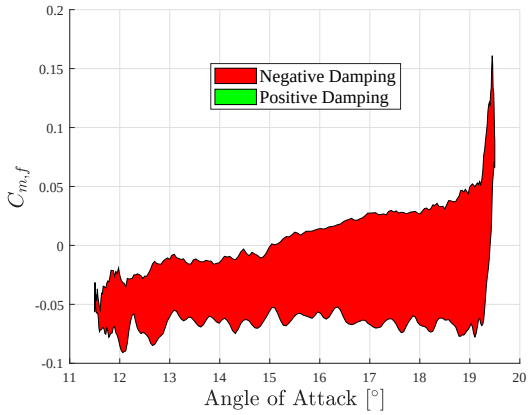

Figure 12. Contribution of the flap to the aerodynamic damping for $K_p = -300$. Dynamic stall with $f = 0.2Hz$ and 8 pressure tap integration scheme

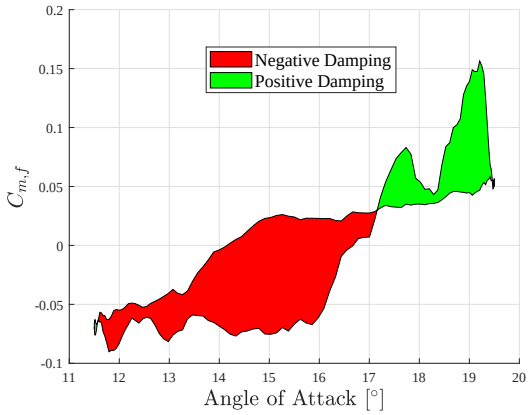

Figure 13. Contribution of the flap to the aerodynamic damping for $K_p = -300$. Dynamic stall with $f = 0.4Hz$ and 8 pressure tap integration scheme

cost of a higher susceptibility to aero-elastic instabilities.

Lastly, the effect of the flap actuation on the dynamic stall onset is quantified in table 3, for the value of K_p that leads to the highest unsteady load reduction. It can be seen that dynamic stall onset is consistently delayed when the flap is actuated. The reason for this is thought to be the increased static stall angle of the airfoil when the flap is actuated upwards, since the detachment of the LEV is thought to be dependent on when that angle is surpassed by the pitching airfoil [10]. Therefore, even though the effect of the flap actuation is small, it does alter the mechanism by which dynamic stall is developed.

Table 3. Phase when Dynamic Stall Onset occurs, for the Baseline Case and the Optimal Smart Rotor Case at different frequencies

	Dynamic stall onset (Phase)		
	0.2Hz	0.4Hz	0.8Hz
Baseline Case	0.18	0.26	0.39
Case with max. reduction in SD_{C_l}	0.19	0.28	0.42

5. Conclusions

A simple proportionate controller acting on the velocity of the flap has been tested for load alleviations purposes. This concept has been proven effective in reducing the unsteady loads generated by a sinusoidal motion of the wing model when dealing with attached flow conditions, with reductions of up to 87.5% in terms of the standard deviation of the C_l. Larger frequencies, and especially larger time lags reduce this value. Therefore, the design of the sensing system should be an integral part in any Smart Rotor concept, so that the time lag is kept to a minimum.

Dynamic stall conditions have also been tested by actuating the model in a sinusoidal motion at an angle of attack close to the static stall angle. The controller is still able to reduce the loads acting on the model, although this reduction drops to around 40%. This stems from the increased range of loads that need to be compensated and the smaller time scale associated

with the detachment of the LEV. Reduced time lag is also shown to improve the performance by reducing the peak-to-peak loads experienced during the detachment of the LEV, and the actuation velocity of the flap is in this case a limiting factor. The load reduction may come at the cost of a deterioration of the aerodynamic damping, and therefore a higher susceptibility to aero-elastic instabilities.

Lastly, the flap actuation influences slightly the development of the dynamic stall cycle, by delaying the onset. This is thought to occur due to the increased α_{ss} of the airfoil when the flap is deflected upwards with respect to no flap actuation.

References

[1] Sieros G, Chaviaropoulos P, Sørensen JD, Bulder BH and Jamieson P 2012 Upscaling wind turbines: theoretical and practical aspects and their impact on the cost of energy *Wind energy* **15(1)** 3-17.
[2] Nijssen RP and Brøndsted P 2013 Fatigue as a design driver for composite wind turbine blades *Advances in Wind Turbine Blade Design and Materials* Woodhead Publishing pp 175-209.
[3] Barlas TK and van Kuik GA 2010 Review of state of the art in smart rotor control research for wind turbines *Progress in Aerospace Sciences* **46** 1-27.
[4] Shipley DE, Miller MS and Robinson MC 1995 Dynamic stall occurrence on a horizontal axis wind turbine blade *National Renewable Energy Laboratory* (Golden, CO)
[5] Corke TC and Thomas FO 2015 Dynamic stall in pitching airfoils: aerodynamic damping and compressibility effects *Annual Review of Fluid Mechanics* 20 **47** 479-505.
[6] Raiola M, Discetti S, Ianiro A, Samara F, Avallone F and Ragni D 2018 Smart rotors: dynamic-stall load control by means of an actuated flap *AIAA Journal* **56(4)** 1388-401.
[7] Moffat RJ 1988 Describing the uncertainties in experimental results *Experimental thermal and fluid science* **1** 3-17.
[8] Carta FO and Niebanck CF 1969 *Prediction of rotor instability at high forward speeds Volume 3. Stall Flutter*
[9] Gerontakos P and Lee T 2006 Dynamic stall flow control via a trailing-edge flap *AIAA journal* **44** 469-80.
[10] Sheng W, Galbraith RM and Coton FN 2006 A new stall-onset criterion for low speed dynamic-stall *Journal of Solar Energy Engineering* **128** 461-71
[11] Brooks T, Marcolini M and Pope D 1984 Airfoil trailing edge flow measurements and comparison with theory, incorporating open wind tunnel corrections *AIAA Journal* **24(8)** 1245-51
[12] McCroskey WJ 1981 The phenomenon of dynamic stall *National Aeronautics and Space Administration* (Moffett Field, CA)
[13] Buhl T, Gaunaa M and Bak C 2005 Potential load reduction using airfoils with variable trailing edge geometry *Journal of Solar Energy Engineering* **127** 503-16
[14] Lackner MA and van Kuik G 2010 A comparison of smart rotor control approaches using trailing edge flaps and individual pitch control *Wind Energy: An International Journal for Progress and Applications in Wind Power Conversion Technology* **13(2-3)** 117-34.
[15] Andersen PB, Henriksen L, Gaunaa M, Bak C and Buhl T 2010 Deformable trailing edge flaps for modern megawatt wind turbine controllers using strain gauge sensors *Wind Energy: An International Journal for Progress and Applications in Wind Power Conversion Technology* **13(2-3)** 193-206.
[16] Bergami L and Poulsen NK 2015 A smart rotor configuration with linear quadratic control of adaptive trailing edge flaps for active load alleviation *Wind Energy* **18(4)** 625-41.
[17] Castaignet D, Barlas T, Buhl T, Poulsen NK, Wedel-Heinen JJ, Olesen NA, Bak C and Kim T. Full-scale test of trailing edge flaps on a Vestas V27 wind turbine: active load reduction and system identification *Wind Energy* **17(4)** 549-64.
[18] Bak C, Gaunaa M, Andersen PB, Buhl T, Hansen P and Clemmensen K 2010 Wind tunnel test on airfoil Risø-B1-18 with an active trailing edge flap *Wind Energy: An International Journal for Progress and Applications in Wind Power Conversion Technology* **13(2-3)** 207-19.
[19] Van Wingerden JW, Hulskamp AW, Barlas T, Marrant B, Van Kuik GA, Molenaar DP and Verhaegen M 2008 On the proof of concept of a 'smart' wind turbine rotor blade for load alleviation *Wind Energy: An International Journal for Progress and Applications in Wind Power Conversion Technology* **11(3)** 265-80.
[20] Van Wingerden JW, Hulskamp A, Barlas T, Houtzager I, Bersee H, van Kuik G and Verhaegen M 2010 Two-degree-of-freedom active vibration control of a prototyped "smart" rotor *IEEE transactions on control systems technology* **19(2)** 284-96.
[21] Bernhammer LO, van Kuik GA and De Breuker R 2016 Fatigue and extreme load reduction of wind turbine components using smart rotors *Journal of Wind Engineering and Industrial Aerodynamics* **154** 84-95.